POLITECNICO DI TORINO
Repository ISTITUZIONALE

Thermal evolution of MnxOy nanofibres as catalysts for oxygen reduction reaction

(Article begins on next page)

02 September 2025

PCCP

Accepted Manuscript

Volume 18 | Number 1 | 7 January 2016 | Pages 1–636

PCCP

Physical Chemistry Chemical Physics
www.rsc.org/pccp

ISSN 1463-9076

ROYAL SOCIETY
OF CHEMISTRY

PERSPECTIVE
Darya Radziuk and Helmuth Möhwald
Ultrasonically treated liquid interfaces for progress in cleaning and separation processes

175 YEARS

ROYAL SOCIETY
OF CHEMISTRY

rsc.li/pccp

Physical Chemistry Chemical Physics

ARTICLE

Thermal evolution of Mn_xO_y nanofibres as catalysts for oxygen reduction reaction

L. Delmondo, *[a] J. A. Muñoz-Tabares,[b] A. Sacco,[b] N. Garino,[b] G. Massaglia,[a,b] M. Castellino,[b] G. P. Salvador,[b] C.F. Pirri,[a] M. Quaglio[b] and A. Chiodoni*[b]

Manganese oxides (Mn_xO_y) are considered as promising catalysts alternative to platinum in fuel cell applications. In fact, a proper catalyst is needed in order to facilitate the Oxygen Reduction Reaction (ORR) at the cathode, and platinum is considered the best one due to its low overpotential for this reaction. Contrary to platinum, Mn_xO_y are inexpensive, environmental friendly and can be shaped in several nanostructures; furthermore, most of them show significant electro-catalytic performance. Several strategies have been carried out in order to increase their efficiency, by preparing light and high-surface area materials. In this framework, nanofibres are among the most promising nanostructures that can be used for this purpose. In this work, a study of the thermal, morphological and catalytic behavior of Mn_xO_y nanofibres obtained through the electrospinning technique is proposed. Emphasis is given to the thermal evolution of the precursors, proposing a possible crystallization mechanism of the different manganese oxides obtained. It turns out that manganese oxide nanofibres exhibit good catalytic performance for the ORR, comparable to those obtained by using Pt-based catalysts.

Introduction

Global warming and finite fossil fuel resources have driven researchers' attention toward green alternatives for energy conversion and storage. In this field, metal air batteries[1] and fuel cells[2] are two of the most investigated topics. At the cathode of these devices, Oxygen Reduction Reaction (ORR) takes place, playing a key role in the definition of their efficiency and, so, in their further improvement. Nevertheless, at ambient conditions, the ORR is not energetically favoured and a proper catalyst is needed in order to lower its overpotential, thus increasing its efficiency. Platinum is the most effective catalyst, carrying out the oxygen reduction via a four-electron reaction pathway. However, Pt is a rare and expensive metal, thus it is not exploitable in large-scale devices. During the last decades, the need for Pt-free catalysts has increased,[3] proposing several alternatives based on metals,[4] carbon,[5] conductive polymers[6] and metal oxides.[7] Among the latter, Transition Metal Oxides (TMOs) have attracted much attention as promising catalysts for ORR,[8] being low-cost, earth-abundant, environmentally friendly and non-toxic materials. Among this variety, manganese oxides gained notable interest for their high catalytic activity toward ORR.

A commonly exploited strategy to increase the efficiency of a catalyst is to enhance its surface area by introducing a nanostructuration. In this way the surface area-to-volume ratio is drastically increased, exposing more catalytic sites to molecular oxygen.[9]

With reference to the mentioned four-electron reaction pathway, many manganese oxides exhibit a number of transferred electrons near to four,[10] which can be influenced by factors such as the valence state[11] of the metal ions, or the type of catalyst structuration.[12] Therefore, a complete analysis aiming at unveiling the relation among the catalytic activity of the manganese oxides and their morphology, structure and composition, would be of great interest.

In the present work, we propose manganese oxide in the form of nanofibres, prepared by means of the electrospinning technique to obtain catalysts with high surface area and reproducible nanostructuration. Based on the aforementioned reasons, nanofibred manganese oxide was fabricated, starting from biocompatible and biodegradable precursors such as polyethylene oxide (PEO), manganese acetate and water. PEO was selected thanks to its biodegradability, being one of the most environmentally friendly polymers that can be used as a templating agents in the nanofibres synthesis. Moreover, it needs only water as a solvent, unlike other common polymers such as polyvinyl pirrolidone (PVP)[13] and polyacrylonitrile (PAN).[14] In addition, PEO has a relatively low decomposition temperature (around 400 °C).

Here we report on the preparation of manganese oxide nanofibres combining the electrospinning technique with a

a. Department of Applied Science and Technology - DISAT, Politecnico di Torino, C.so Duca degli Abruzzi 24, 10129 Torino (Italy).

b. Center for Sustainable Future Technologies @PoliTo, Istituto Italiano di Tecnologia, C.so Trento 21, 10129 Torino (Italy).

* Corresponding authors Angelica Chiodoni and Luisa Delmondo. Tel.: + 39 011 5091 902/931; Fax: +39 011 5091901; e-mail: angelica.chiodoni@iit.it, luisa.delmondo@polito.it.

ARTICLE

subsequent thermal treatment. Morphology and composition differences will be highlighted at different calcination temperatures, proposing a possible conversion mechanism and thus accounting for the obtained crystalline phase and morphology. Following an experimental approach reported in several works in the literature,[10,15-19] the catalytic behaviour of the different nanostructured fibres has been evaluated through the Rotating Ring Disk Electrode (RRDE) electrochemical measurements, commented and compared with reference to the Pt catalyst.

Experimental

Materials

Polyethylene oxide (molecular weight M_w = 600 kDa), manganese (II) acetate tetrahydrate ($Mn(CH_3COO)_2 \cdot 4H_2O$), ethanol, 2-propanol, Nafion solution (5 wt% in water and aliphatic alcohols), potassium hydroxide and Pt/C paste were all purchased from Sigma-Aldrich and processed without any further purification. Silicon wafers (p type <100>, 1-30 $\Omega \cdot$cm) were supplied by MEMC. De-ionized water (Di-water) was used as solvent.

Manganese oxide nanofibres synthesis

The starting polymeric solution, named 5%PEO+MnAc, was prepared by mixing 9 ml 5wt% of aqueous PEO solution with 3 ml of 20 wt% aqueous manganese acetate solution, and left under stirring for 24 h at ambient temperature. Afterwards, the polymeric solution was loaded in a 6 ml syringe, connected to a stainless steel needle (27 Gauge x 15 mm) and mounted into a NANON 01A electrospinning apparatus (MECC CO., LTD.) equipped with a high voltage power supply (HVU-30P100) and a syringe pump setup operating with a flow rate ranging from 0.1 ml/h up to 99.9 ml/h. During the electrospinning process, a voltage of about 14.5 kV was applied between the needle and the planar collector plate, set at a distance of 10 cm. The collector plate was covered with a silicon substrate, selected in order to easily perform structural and morphological analysis on the nanofibres mats.

The electrospun 5%PEO+MnAc nanofibres were calcined in air by means of a vertical furnace (Carbolite, VST 12/300/3216) for 3 h in air, with a heating rate of 2.5 °C/min at three different final temperatures (475 °C, 600 °C and 725 °C). All the final calcination temperatures ensured the complete decomposition of the PEO and the manganese acetate oxidation. A sample of the as-electrospun fibres was left uncalcined for the in-situ XRD experiment.

Characterizations

Decomposition behaviours of 5%PEO, MnAc and 5%PEO+MnAc were analysed by means of thermogravimetric analysis (TGA) under an air flux at a constant scan rate of 10 °C/min, using a TG209 F1 Libra from Netzsch. All the measurements were performed under air flux, up to a temperature of 800 °C.

In situ X-ray diffraction was performed in order to investigate the temperature dependence of the oxidation process during the calcination of the manganese acetate. The spectra were recorded in Bragg–Brentano symmetric geometry by using a PANalytical X'Pert Pro instrument (Cu-K radiation, 40 kV and 40 mA) equipped with an X'Celerator detector and a XRK 900 Reactor Chamber used as furnace heater. The samples were heated in air up to 475 °C, 600 °C and 725 °C at a heating rate of 2.5 °C/min, acquiring the spectra at steps of 50 °C (continuous scan mode) in the range of 10° to 68° and 0.02° as step size.

The morphologies of all samples were examined by means of Field Emission Scanning Electron Microscopy (FESEM, ZEISS, Auriga and Supra 40). All the FESEM images were collected with an in-lens detector, at 5 kV and using a bean current of about 330 pA (aperture size 30 μm).

Transmission Electron Microscopy (TEM) observations were performed with a FEI Tecnai F20ST, equipped with a field emission gun (FEG), operating at 200 kV. Samples for TEM were prepared by suspending a small quantity of scratched nanofibres in ethanol, subsequently immersed in ultrasonic bath. A drop of the suspension was then drawn and put on a standard TEM holey carbon copper grid, analysing the specimen after the complete evaporation of the solvent.

The electrochemical measurements were carried out through a CHInstrument 760D electrochemical workstation and an ALS RRDE-3A rotating ring disk electrode apparatus in a four-electrodes electrochemical cell, constituted by a glassy carbon disk/Pt ring working electrode, a Pt counter electrode and a Ag/AgCl reference electrode; 0.1 M KOH aqueous solution was used as electrolyte.

Manganese oxide catalysts were deposited on the glassy carbon disk according to the following method: 2 mg of catalyst were dispersed in a solution containing 25 μl of water, 175 μl of Nafion© solution and 100 μl of 2-propanol (from Sigma-Aldrich). The mixture was ultrasonicated for 2 minutes in order to obtain a uniform black dispersion; then 10 μl of this formulation were cast-coated onto the disk surface and then let drying at room temperature for one day. Commercial Pt/C paste (Sigma-Aldrich) was used as reference catalyst; the deposition was carried out as already described. For all the analysed materials, the final catalyst loading was 0.5 mg/cm^2.

RRDE measurements were performed by cathodically scanning the disk electrode in the range -0.2 ÷ -0.8 V vs Ag/AgCl, with fixed scan rate (5 mV/s) and rotating speed (2500 RPM), while maintaining the ring electrode potential at 0.2 V, and simultaneously acquiring ring I_R and disk I_D currents. Electron transfer number n and peroxide percentages $HO_2^-\%$ were calculated according to the formulas[20]:

$$n = 4 \cdot \frac{I_D}{I_D + I_R/N} \tag{1}$$

$$HO_2^-\% = 200 \times \frac{I_R/N}{I_D + I_R/N} \tag{2}$$

Journal Name ARTICLE

where N is the current collection efficiency of the Pt ring. Electrochemical Impedance Spectroscopy (EIS) measurements were carried out with the same electrochemical workstation at -0.3 V vs Ag/AgCl potential and 2500 RPM rotating speed, with a AC signal of 10 mV amplitude and $10^{-2} - 10^{4}$ Hz frequency range.

Results and discussion

Thermal analysis

Thermo-Gravimetric Analysis (TGA) was performed on 5 wt% PEO water-based solution, analysed after the initial complete removal of the water content by means of a vacuum pump (name of the sample: "5%PEO-dried"), on manganese acetate salt, analysed without any further treatment (name of the sample: "MnAc"), on 5wt%PEO+manganese acetate solution, analysed after its drying (name of the sample: "5%PEO+MnAc-dried"), in order to study their thermal behaviour.

In Fig. 1 the results of the TG analysis of 5%PEO-dried, MnAc and 5%PEO+MnAc-dried are reported. In order to more easily put in evidence the key temperatures for each material and component, the derivatives of the TGA curves are calculated and reported by dotted lines in Fig. 1. The 5%PEO-dried black curves in Fig. 1 clearly show the almost complete degradation of the polymer within 450 °C. The red curves show the thermal evolution of MnAc, highlighting different decomposition steps. The first occurs at around 100 °C, and corresponds to a weight loss of 30%, in which the acetate salt completely loses the coordinated water molecules. A second step occurs at around 300 °C, corresponding to the transformation of manganese acetate into manganese oxyacetate ($MnOCH_3COO$) and/or manganese hydroxyacetate ($Mn(OH)CH_3COO$), as suggested in the literature.[21,22] A final exothermic process follows at around 320 °C: starting from 350 °C, all the acetate component is completely degraded and the manganese oxyacecate or hydroacetate is entirely transformed into manganese oxide,[22] leaving a black/brown residue in the TGA alumina crucible.

The thermal evolution of 5%PEO+MnAc-dried, represented by the blue curves in Fig. 1, appears similar to the MnAc one (red curve). In fact, the corresponding degradation steps take place almost at the same temperatures range. As already said, at around 100 °C, the acetate component loses the coordinated water molecules. The second step occurs between 250 °C and 400 °C and corresponds to the mixed thermal decomposition of PEO and manganese acetate. As showed in the blue curve, starting from 400 °C, the PEO component is completely degraded, leaving manganese oxide only, with black/brown residue in the TGA alumina crucible.

Structural characterization

In order to investigate the crystallization process of the as-electrospun 5%PEO+MnAc nanofibres as a function of the temperature, *in-situ* X-ray diffraction was carried out in a reaction chamber. This study is of particular relevance, because it defines a correlation between the morphological and electrochemical behaviour of the calcined nanofibres, with the specific manganese oxide crystalline phase. Fig. 2 shows the XRD spectra acquired during the calcination in air, and collected starting from ambient temperature up to 725 °C, at steps of 50 °C. The selection of the calcination temperatures was done on the basis of the TGA characterization.

As a first comment, the spectrum at 25 °C shows two main peaks at 19.20° and 23.41°, related to the initial PEO component,[23] that disappears in the curve collected at 75 °C, being the PEO melting point at 65 °C.

Starting from 125°C it can be clearly noticed the appearance of four main peaks, at about 36.1°, 32.2°, 59.7° and 28.8° (in order of decreasing intensity), corresponding to the (211), (103), (224) and (112) planes of Mn_3O_4 (Hausmannite, JCPDS 00-024-0734), respectively. The broadness of these peaks witnesses the very small crystal size. By increasing the temperature, such peaks become sharper and more defined, giving evidence of a crystal size increase. The Mn_3O_4 phase remains almost the single present crystalline phase up to 525 °C.
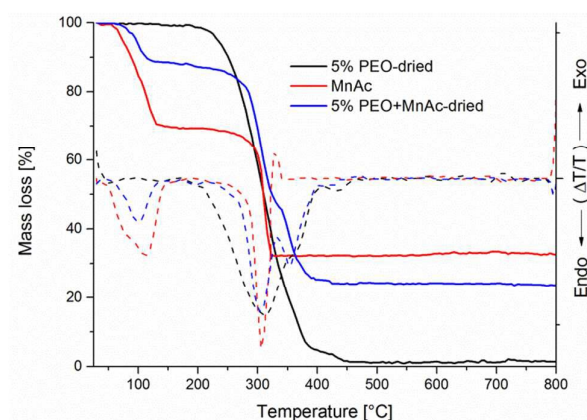

Figure 1: TGA curves for the different samples (straight curves, left axis): 5%PEO-dried (black curve), MnAc (red curve) and 5%PEO+MnAc-dried (blue curve). First derivatives of the TGA curves (dashed curves, right axis) with the same colour code.
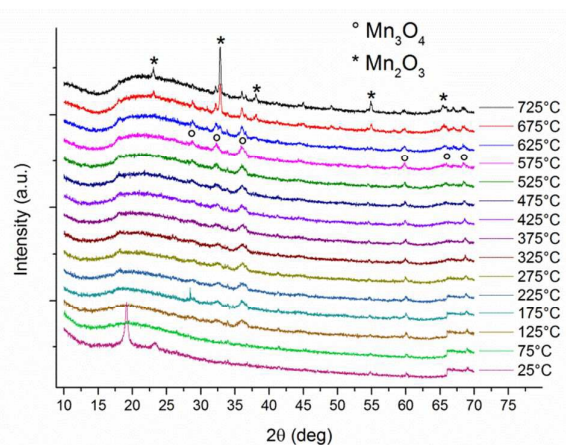

Figure 2: In-situ XRD spectra of the 5%PEO+MnAc nanofibres collected with the reactor chamber from 25 °C to 725 °C, at steps of 50 °C.
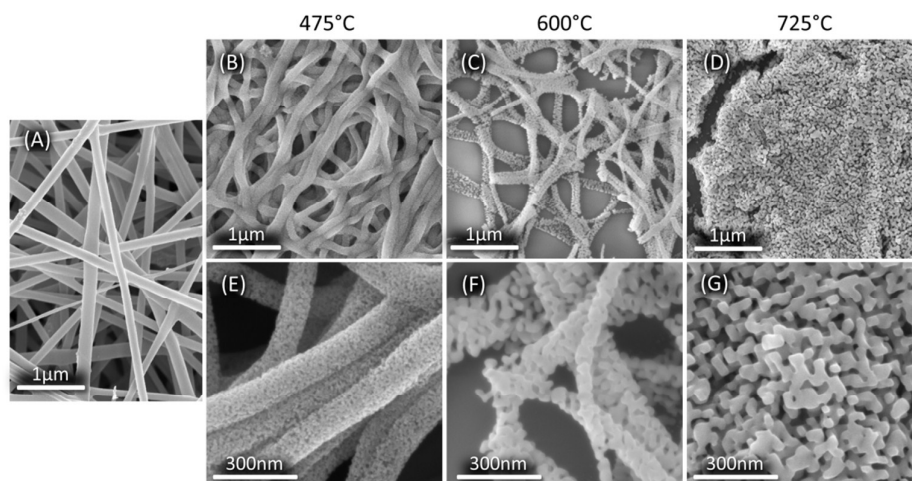
ARTICLE

475°C   600°C   725°C

Figure 3: FESEM images of the as-electrospun (A) and calcined nanofibres (B-G) at different magnifications. The manganese oxide nanofibres are calcined at different final temperatures: (B) and (E) at 475 °C, (C) and (F) at 600 °C, (D) and (G) at 725 °C.

Between 575 °C and 625 °C, the formation of a second phase starts to appear to the detriment of Mn_3O_4, that progressively disappears as the temperature arises. This second phase is identified as Mn_2O_3, as shown by the presence of five main peaks at 32.7°, 55.1°, 23.2°, 38.1°, and 65.5° (in order of decreasing intensity) corresponding to the (222), (440), (211), (400) and (622) planes of Mn_2O_3 (Bixbyite, JCPDS 00-041-1442), respectively. The Mn_2O_3 phase is characterized by very sharp peaks, putting evidence of the formation of bigger crystals, as better discussed in the next paragraph.

Morphological characterization

Scanning and Transmission Electron microscopies were carried out on three samples calcined in air in a tubular oven at three different temperatures: 475 °C, 600 °C and 725 °C. Based on

the in-situ XRD spectra, the first temperature has been selected in order to analyse the morphology and the crystalline characteristics of pure Mn_3O_4, the second has been selected because it represents a temperature in which there is the co-presence of the two manganese oxides, and the third one because at this temperature the sample is nearly pure Mn_2O_3.

In Fig. 3 the FESEM images of the as-electrospun and calcined nanofibres at different magnifications are presented. Fig. 3(A) reports the uncalcined nanofibres, already described and discussed elsewhere.[8] Fig. 3(B and E) show the nanofibres calcined at 475 °C, Fig. 3(C and F) show the nanofibres calcined at 600 °C, while and Fig. 3(D and G) show the nanofibres calcined at 725 °C.

As a general comment, it turns out that the calcination temperature strongly influences not only the nanocrystals shape and size, as already discussed for the in-situ XRD

475°C   600°C   725°C
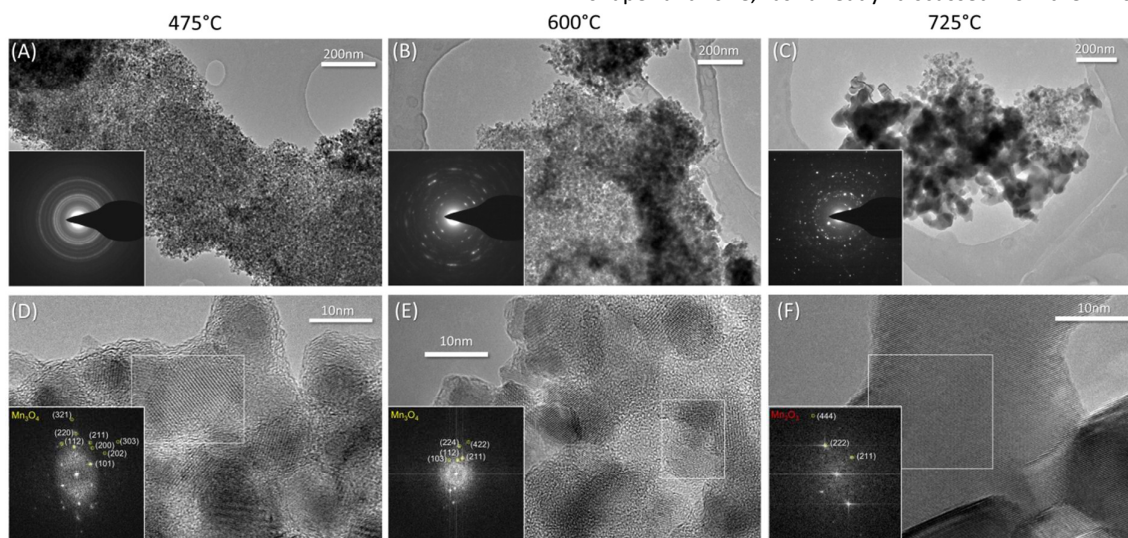
Figure 4: TEM images of the manganese oxide nanofibres calcined at different final temperatures: (A) and (D) at 475 °C, (B) and (E) at 600 °C, (C) and (F) at 725 °C. In the first row (panels A, B, C), low magnification images and electron diffraction patterns put in evidence the change in the crystalline phase and morphology, as the calcination temperature increases. In the second row (panels D, E, F), higher magnifications and FFT of small regions , are reported.

ARTICLE

Figure 5: Possible mechanism for the formation of the Mn_3O_4 nanocrystals inside the nanofibres and their evolution into Mn_2O_3.

characterization, but also the fibre shape. In fact, by looking at Fig. 3, it appears clear that the nanofibres are able to retain a 1D shape in a quite lar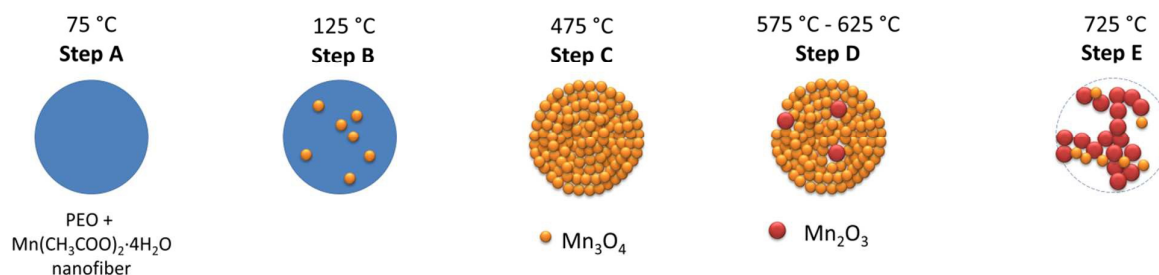ge range of temperatures (from ambient temperature up to 525 °C). Nevertheless, when Mn_2O_3 starts to nucleate, above 575 °C, the crystals are bigger than those of the initial nucleation of Mn_3O_4. When the final calcination temperature is reached, the Mn_2O_3 crystals are so big that the nanostructuration into fibres is not anymore retained, leaving a nanostructured film of manganese oxide. These findings are in line with what observed in the in-situ XRD spectra.

In Fig. 4 the TEM images and the electron diffraction patterns of the nanofibres calcined at the three different temperatures are presented. Fig. 4(A and D), Fig. 4(B and E) and Fig. 4(C and F) show the nanofibres treated at 475 °C, 600 °C and 725 °C, respectively. The insets of Fig. 4(A-B-C) are the electron diffraction pattern, collected at the same conditions for the three samples. The insets of Fig. 4(D-E-F) represent the Fast Fourier Transform (FFT) of the squared white regions in the same figures.

At 475 °C (Fig. 3(E), 4(A-D)), the manganese oxide nanofibres are constituted by very small crystals (in the range of 5-10 nm) of pure Mn_3O_4. The rings in the electron diffraction pattern in the inset of Fig. 4(A) show a randomly oriented pattern of many small crystals. At 600 °C (Fig. 3(F), 4(B-E)), the nanofibres are slightly discontinuous and are characterized by bigger crystals (in the range of 10-20 nm). The electron diffraction pattern still evidences the presence of rings, but in this case there are some intense spots that indicate the co-presence of small and big crystals, in agreement with in-situ XRD. When the calcination temperature reaches 725 °C (Fig. 3(G)), the shape of the nanofibres is no more retained, and they are mostly composed by Mn_2O_3, with big crystals (in the range of 40-200 nm) in a dendritic arrangement (see Fig. 3(G)). In Fig. 4(C) it is reported, for sake of comparison, a small part of the fibres in which, beside the main big Mn_2O_3 crystals, there are also smaller Mn_3O_4 crystals. The high-magnification of one of the big crystals (Fig. 4(F)) show that they are almost monocrystalline, in agreement with XRD.

Crystal formation and evolution

Based on the experimental observations, a possible mechanism for the formation of the Mn_3O_4 nanocrystals and their evolution into Mn_2O_3 can be derived,[13] as depicted in Fig. 5. At 75 °C the 5%PEO+MnAc nanofibres are completely

amorphous (step A in Fig. 5) as demonstrated by the XRD spectrum in Fig. 2. When the temperature is increased, Mn_3O_4 nanocrystals start to nucleate in the amorphous PEO polymeric matrix. At 125 °C, the PEO acts as a support during the initial two steps (step B in Fig. 5), keeping isolated the growing nanocrystals. After the complete degradation of the PEO, at 475 °C, the nanofibres are constituted by Mn_3O_4 nanocrystals only, which are enough interconnected and sufficiently large to retain the 1D shape (step C in Fig. 5).

By further increasing the calcination temperature, Mn_2O_3 starts to nucleate between 575 °C and 625 °C following the reaction:[18]

$$4\ Mn_3O_4 + O_2 \rightarrow 6\ Mn_2O_3 \tag{3}$$

Based on the previous reaction, Mn_3O_4 is thermodynamically favoured to be transformed into Mn_2O_3 in the presence of oxygen or air,[24] as in this case. In fact, during the coordination with oxygen, Mn_3O_4 crystals coalesce, resulting in the formation of the Mn_2O_3, characterized by bigger crystals (stage D in Fig. 5).

Further increasing the temperature up to 725 °C (stage E in Fig. 5), Mn_3O_4 continues to be converted. Moreover, Mn_2O_3 grows in crystal size, assuming a dendritic conformation and destroying the initial nanofibred shape, with only a residual small amount of the Mn_3O_4 in the sample. It is reasonable to suppose that with a further increase of temperature, all the Mn_3O_4 crystals would be completely converted in Mn_2O_3.

Catalytic performance

The catalytic performance of the different samples was evaluated through RRDE technique, whose results are reported in Fig. 6(A). As clearly evident, nanofibres calcined at 600 °C, i.e. composed by a mixed phase composition, show reduced activity with respect to samples exhibiting pure phases. In fact, a valuable dependency on the potential can be observable for both electron transfer number and peroxide percentage curves, with values in the range 3.26 ÷ 3.46 and 27 ÷ 37 %, respectively. On the contrary, quite constant values were obtained for samples treated at 475 °C (about 3.66 and 17 %) and at 725 °C (about 3.69 and 16 %). Based on these results, it can be asserted that electrospun nanofibres show performances in line or even better with respect to Mn-based[16] or other cost-effective ORR catalysts recently proposed in the literature.[17,25,26] The nanofibres show indeed
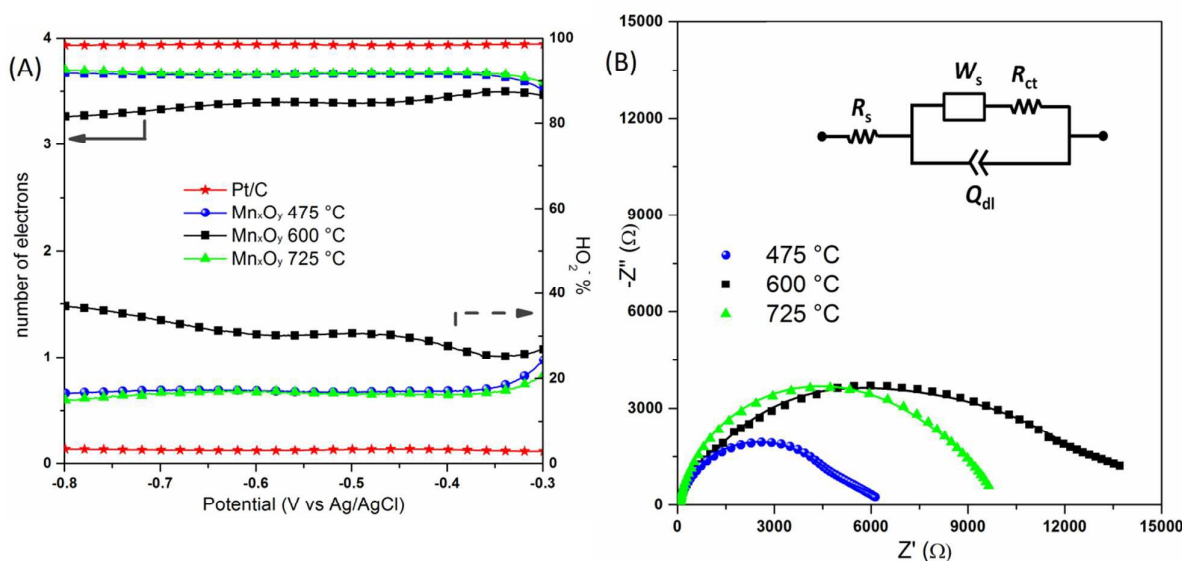
ARTICLE

Journal Name

Figure 6: (A) Comparison of electron transfer number (left axis) and peroxide percentage (right axis) evaluated from RRDE measurements of the different manganese oxide-based samples and of the reference Pt/C catalyst. (B) Nyquist plot of the impedance of the different samples. The points are experimental data while the continuous lines are the curves obtained from a fitting procedure using the equivalent circuit shown in the inset.

comparable performance with respect to expensive Pt-based materials, as demonstrated in Fig. 6(A). In addition, it is worth nothing that, despite different phase compositions and morphologies, the catalytic activity of the samples calcined at 475 °C and 725 °C is rather similar. In order to cast light on this aspect, EIS analysis was carried out; Nyquist plots related to the three samples under investigation are reported in Fig. 6(B). All the three spectra exhibit a high-frequency arc which is related to the charge transfer at the electrode/electrolyte interface, and a low-frequency side arc related to the diffusion of species; the displacement between the origin of axis and the beginning of high-frequency arc accounts for the electrolyte resistance.[27] Apart from mixed-phase nanofibres, characterized by largest impedance values, pure Mn_3O_4 sample exhibit reduced resistance with respect to Mn_2O_3 one; however, the latter is characterized by lower capacitive behaviour, as manifest from the higher Z'' values, roughly proportional to the inverse of capacitance.[28] In order to quantitatively evaluate resistances and capacitances associated with the pure and mixed phases nanofiber samples, EIS data were fitted with the Randles' equivalent circuit[29] shown in the inset of Fig. 6(B). In accordance with the above reported qualitative analysis, the following values were obtained for the charge transfer resistances R_{ct}: 6492 Ω, 14080 Ω and 10694 Ω for samples calcined at 475 °C, 600 °C and 725 °C respectively. For what concerns double layer capacitances (here modelled through constant phase elements[30] with exponents β in the range 0.88 ÷ 0.91), values of 12.1, 6.4 and 6.1 $s^\beta/Ω$ were obtained for the three samples. As discussed in the morphological characterization section, the sample calcined at 475 °C is characterized by small Mn_3O_4 crystals and a good preservation of the fibre shape, thus offering a larger surface area exposed to the electrolyte while ORR takes place, if compared with the sample treated at 725 °C (composed by

big crystals of Mn_2O_3 and a partial loss of the fibre nanostructuration). This implies a higher number of active sites available for the reduction process in Mn_3O_4 with respect to the other sample (Mn_2O_3), and this could explain the observed lower value of the charge transfer resistance. On the other hand, larger exposed surface areas involve also larger capacitances, since double layer capacitor values are directly proportional to contact areas; this consideration is in agreement with the obtained results. Starting from the calculated electrical parameters, characteristic time constant associated to the charge transfer process can be obtained using the formula[31] $\tau = (R_{ct}Q_{dl})^{1/\beta}$: similar values equal to 0.51 and 0.48 s were obtained for pure Mn_3O_4 and pure Mn_2O_3 samples, respectively. Such results imply that even if the charge transfer resistance is reduced for the nanofibres calcined at lower temperature (475 °C), the larger capacitive behaviour exhibited by this sample is detrimental for the whole activity, leading to efficiencies which are comparable with that of Mn_2O_3 fibres. These findings once again support the hypothesis that the crystalline structure is not the only parameters to take into account when evaluating the catalytic activity of manganese oxide-based materials but also the morphology and nanostructuration of the crystals should be considered and optimized for the reduction reaction.

Conclusions

Manganese oxide nanofibres were prepared starting from biocompatible and biodegradable precursors, by means of the electrospinning technique. In particular, with the in-situ XRD it was possible to define the onset temperature at which Mn_3O_4 and Mn_2O_3 start to crystallize, i.e. 125 °C and about 600 °C, respectively. In the range of 475-575 °C a single phase catalyst (Mn_3O_4) was obtained without any polymeric template residue

and retaining the initial nanofibred shape, with a progressive increase of the crystal size with temperature. Furthermore, it was demonstrated that a coalescence phenomenon occurs during the transformation of Mn_3O_4 into Mn_2O_3 in the temperature range 575-625 °C. This is detrimental for the initial nanostructure, leading to a dendritic structure mostly composed of Mn_2O_3.

Good catalytic performances for the oxygen reduction reaction were highlighted for the three Mn_xO_y compositions considered. In particular, pure Mn_3O_4 and Mn_2O_3 showed significant *n* values around 3.7, at potentials lower than -0.4 V, which is in line with other cost-effective catalysts proposed in the literature, resulting to be good candidates as low-cost and green catalysts to be integrated with electrodes for applications in electrochemical devices.

Conflicts of interest

There are no conflicts of interest to declare.

References

1   N. Ortiz-Vitoriano, N. E. Drewett, E. Gonzalo, T. Rojo, *Energy Environ. Sci.*, 2017, **10**, 1051-1074.
2   C. Zhang, P. Liang, X. Yang, Y. Jiang, Y. Bian, C. Chen, X. Zhang, X. Huang, *Biosens. Bioelectron*., 2016, **81**, 32–38
3   Z.-Y. Zhou, N. Tian, J.-T. Li, I. Broadwell and S.-G. Sun, *Chem. Soc. Rev.*, 2011, **40**, 4167–4185.
4   C. Santoro, A. Serov, L. Stariha, M. Kodali, J. Gordon, S. Babanova, O. Bretschger, K. Artyushkova and P. Atanassov, *Energy Environ. Sci.,* 2016, **9**, 2346–2353.
5   S. Ratso, I. Kruusenberg, M. Kaarik, M. Kook, R. Saar, M. Pars, J. Leis, K. Tammeveski, *Carbon*, 2017, **113,** 159-169.
6   Q. Zhou and G. Shi, *J. Am. Chem. Soc.*, 2016, **138**, 2868–2876.
7   N. Garino, A. Sacco, M. Castellino, J.A. Munoz-Tabares, M. Armandi, A. Chiodoni, C.F. Pirri, *ChemistrySelect*, 2016, **1**, 3640 – 3646.
8   L. Delmondo, G. P. Salvador, J. A. Munoz-Tabares, A. Sacco, N. Garino, M. Castellino, M. Gerosa, G. Massaglia, A. Chiodoni, M. Quaglio, *Appl. Surf. Sci.*, 2016, **388**, 631–639.
9   H.A. Gasteiger, S.S. Kocha, B. Sompalli, F.T. Wagner, *Appl. Catal. B*, 2005, **56**, 9–35.
10 K. A. Stoerzinger, M. Risch, B. Han and Y. Shao-Horn, *ACS Catal*., 2015, **5**, 6021−6031.
11 F.H.B. Lima, M.L. Calegaro, E.A. Ticianelli, *J. Electroanal. Chem.*, 2006, **590**, 152–160.
12 W.Xiao, D. Wang and X.W. Lou, *J. Phys. Chem. C*, 2010, **114**, 1694–1700.
13 G. Yang, W. Yan, J. Wanga and H. Yang, *Cryst. Eng. Comm.*, 2014, **16** , 6907–6913.
14 Y. Du, X. Zhao, Z. Huang, Y. Li and Q. Zhang, *RSC Adv.*, 2014, **4**, 39087–39094.
15 R. Burkitt, T.R. Whiffen, E.H. Yu, *Appl. Catal. B: Environ*., 2016, **181**, 279-288.
16 S. Bag, K. Roy, C.S. Gopinath and C.R. Raj, *ACS Appl. Mater. Interfaces*, 2014, **6** (4), 2692–2699.
17 X. Liu and W. Hu, *RSC Adv.*, 2016, **6**, 29848-29854.
18 X.B. Gong, S.L. You, X.H. Wang, J.N. Zhang, Y. Gan and N.Q. Ren, *Biosens. Bioelectron*., 2014, **55**, 237-241.
19 Y. Xue, W. Jin, H. Du, S. Wang, S. Zheng and Y. Zhang, *RSC Adv.*, 2016, **6**, 41878-41884.
20 A. Sacco, N. Garino, A. Lamberti, C. F. Pirri, M. Quaglio, *Appl. Surf. Sci.*, 2017, **412**, 447-454.
21 M.A. Mohamed, S.A. Halawy, *Thermochim. Acta*, 1994, **242**, 173- 186.
22 A.K.H. Nohaman, H.M. Ismail, G.A.M. Hussein, *J. Anal. Appl. Pyrol.*, 1995, **34**, 265-278.
23 A. Chandra, R.C. Agrawal and Y.K. Mahipal, *J. Phys. D: Appl. Phys.*, 2009, **42**, 135107
24 A. N. Grundy, B. Hallstedt and L. J. Gauckler, *J. Phase Equilib.*, 2003, **24**, 21–39.
25 E.A. González , M. Gulppi, M.A. Páez. A, J.H. Zagal, *Diamond Relat. Mater.*, 2016, **64**, 119-129.
26 S.A. Wohlgemuth, R.J. White, M.G. Willinger, M.M. Titirici and M. Antonietti, *Green Chem.*, 2012, **14**, 1515-1523.
27 A. Sacco, A. Lamberti, M. Gerosa, C. Bisio, G. Gatti, F. Carniato, N. Shahzad, A. Chiodoni, E. Tresso, L. Marchese, *Sol. Energy*, 2015, **111**, 125-134.
28 A. Sacco, *Renew. Sustain. Energy Rev.*, 2017, **79**, 814-829.
29 J.E.B. Randles, *Discuss. Faraday Soc.*, 1947, **1**, 11-19.
30 M.E. Orazem and B. Tribollet, *Electrochemical Impedance Spectroscopy*, John Wiley & Sons, Inc., Hoboken, NJ, USA, 2008.
31 F. Bella, E. D. Ozzello, A. Sacco, S. Bianco, R. Bongiovanni, *Int. J. Hydrogen Energy*, 2014, **39**, 3036–3045.

Physical Chemistry Chemical Physics Accepted Manuscript

Table of contents of:

Thermal evolution of Mn$_x$O$_y$ nanofibers as catalysts for oxygen reduction reaction

L. Delmondo, *[a] J. A. Muñoz-Tabares,[b] A. Sacco,[b] N. Garino,[b] G. Massaglia,[a,b] M. Castellino,[b] G. P. Salvador,[b] C.F. Pirri,[a] M. Quaglio[b] and A. Chiodoni*[b]

[a.] Department of Applied Science and Technology - DISAT, Politecnico di Torino, C.so Duca degli Abruzzi 24, 10129 Torino (Italy).
[b.] Center for Sustainable Future Technologies @PoliTo, Istituto Italiano di Tecnologia, C.so Trento 21, 10129 Torino (Italy).
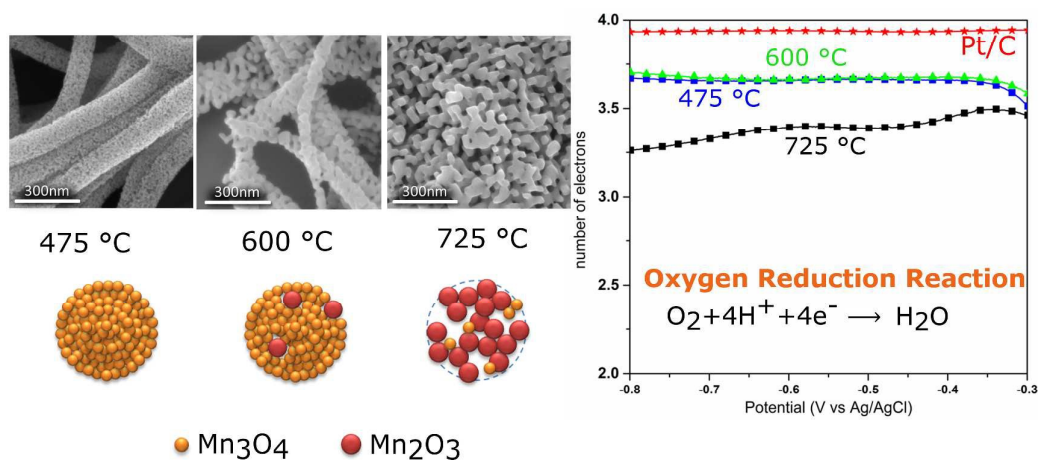
New insight into physical chemistry

The present study shows how, starting from green and low-cost precursors, nanostructured manganese oxides with good catalytic efficiencies for oxygen reduction reaction, can be fabricated, through a technique, the electrospinning, able to create a hierarchical nanostructuration of the material. Furthermore the present paper put in evidence how the fine-tuning of the crystalline phase and morphological features, and thus the fine-tuning of the surface properties, influences the electro-catalytic behaviour of the different prepared catalysts.